Sci. Rep. Kanazawa Univ.
Vol. 62, pp. 37–49, 2018

ARTICLES

Fermi level smearing effect in the perpendicular interface Fe/MgO magnetic anisotropy

Nurul IKHSAN[1,2]*, Indra PARDEDE[1,3], Tomosato KANAGAWA[1], Daiki YOSHIKAWA[1], and Tatsuki ODA[1,4]

[1]Graduate School of Natural Science and Technology, Kanazawa University, Kakuma, Kanazawa, Ishikawa 920-1192, Japan
[2]School of Computing, Telkom University, Bandung 40257, Indonesia
[3]Department of Physics, Institut Teknologi Sumatera, Lampung 35365, Indonesia
[4]Institute of Science and Engineering, Kanazawa University, Kakuma, Kanazawa, Ishikawa 920-1192, Japan

(Received June 25, 2018 and accepted in revised form August 28, 2018)

Abstract Effects of the Fermi level smearing introducing temperature dependence of energy-band occupation numbers were investigated in terms of magnetic anisotropy by using a density functional theory. In a perpendicular magnetization film Fe(0.7nm)/MgO, the magnetocrystalline anisotropy shows a decrease with respect to the smearing temperature; 0.4mJ/m^2 from 11K to 527K. This reduction is not negligible and is expected to partially compensated by a reduction in the shape magnetic anisotropy, assuming reasonable values of the Curie temperature and saturated magnetic moment. The resulting temperature dependences in the total perpendicular magnetic anisotropy energy is in agreement with those of available experimental data semi-quantitatively.

Keywords. Magnetocrystalline anisotropy, Shape anisotropy, First-principles electronic structure calculation, Density functional theory

1 Introduction

Perpendicular magnetic anisotropy (PMA) has an important role for designs of better devices of spin transfer torque recording magnetoresistive random access memory (STT-MRAM) [1, 2]. In the approaches of both theory and experiment, a lot of progress has been made for developing functionals or improving performances [3–12]. The properties of temperature dependence in PMA are highly requested for designing ferromagnetic magnetic materials. Recently, the experimental work by Xiang *et al.* showed a temperature effect of perpendicular magnetic anisotropy. This effect is a reduction of 0.15 mJ$/$m^2 in the case that the temperature decreases form 300K to 10K [10]. This work motivates us to investigate temperature effects by theoretical approach. Up to now, there are many works of theoretical approach for the systems of localized magnetic moments (single ion-magnetic anisotropies) [13–15]. In these approaches, the magnetic anisotropy energy (K) was

*Corresponding author Email: ikhsan@cphys.s.kanazawa-u.ac.jp

treated as a cubic polynomial function of magnetization (M). For the metallic epitaxial films, a square function was employed at the low temperature [16,17]. The theoretical approaches showed that K is proportional to M^2 in case of $L1_0$-ordered FePt [18, 19]. The recent density functional approach to disordered magnetic bulk alloys explains an anomalous temperature dependence of magnetocrystalline anisotropy [20].

For the design of materials in emerging nanoscale memory and logic device, Alzate *et al.* showed that in the system MgO/CoFeB/Ta-based MTJ [21], M as temperature dependence fitted well with the Blöch law ($T^{3/2}$) [22]. In addition to this, K as temperature dependence fitted well with a power law of M^2 or similar one. Wen *et al.* also showed a similar behavior of temperature dependence on M and K in Ru/Co_2FeAl/MgO-based MTJ [23]. For the thinner films of several iron monolayers, the temperature dependence of M was implied to change from $T^{3/2}$ to T^2 [24].

In the materials for perpendicular-MRAM devices, the property of PMA is mainly ascribed to spin-orbit coupling (SOC) in the metallic electronic structure. The magnetocrystalline anisotropy for metal has been estimated successfully since the 1980's using density functional approaches. The PMA of thin films has qualitatively or semi-quantitatively been explained. This is a consequence of the fact that the PMA from SOC overcomes the magnetic shape anisotropy (SA) which favors in-plane magnetization. The latter contribution to magnetic anisotropy has been investigated for a long time, including its temperature-dependent property. However, the temperature dependence of the magnetic anisotropy caused by metallic energy bands has not been investigated very well, particularly for thin film systems.

In the present work, we investigated smearing effects on the Fermi level in terms of the magnetic anisotropy energy of the metal slab system for magnetic devices, by means of a first-principles calculation. These effects are expected to contribute to a temperature dependence in the magnetic anisotropy caused by SOC. In combination with SA analyses, a saturating behavior in K at room temperatures may be comprehended, compared with the available experimental data [10].

2 Method

2.1 General theory

Finite temperature effects can be taken into account in the band-energy by the Mermin's approach [25]. In such kind of approaches a set of temperature-dependent electron occupations is introduced. Using an analogy of quasi-one-particles, the total Hamiltonian of system H can be divided into two parts; $H = H_0 + \Delta H$, where H_0 and ΔH represent quasi-one-electron's part and the other part, respectively. Schrödinger equation for H_0 is represented as follow: $H_0\varphi_i = \varepsilon_i\varphi_i$, where ε_i and φ_i are the eigenvalue and eigenwavefunction. ΔH contains all interactions between quasi-one-electrons. The free energy of system at the temperature T is expressed as follows:

$$F_{\rm tot} = \sum_i f_i(\varepsilon_i - \mu) - k_{\rm B}TS + \Delta F + \mu N_e\,, \tag{2.1}$$

$$\Delta F = -k_{\rm B}T\log{\rm Tr}\left[\exp\{-\Delta H/k_{\rm B}T\}\right], \tag{2.2}$$

where N_e and μ are the number of electrons and chemical potential, f_i is the occupation number of band energy, defined as $f_i = 1/[\exp\{(\varepsilon_i - \mu)/k_{\rm B}T\} + 1]$. Note that $\sum_i f_i = N_e$. The second term in Eq. (2.1) represents the entropic energy of non-interacting one-particles and $S = \sum_i s_i = \sum_i y(f_i)$, where $y(x) = -\{x\log x + (1-x)\log(1-x)\}$. The third term ΔF in Eq. (2.1) represents the contributions from all the other interactions between electrons which are not included in the first (one-particle) term. Ferromagnetism is stabilized by an exchange magnetic field (molecular

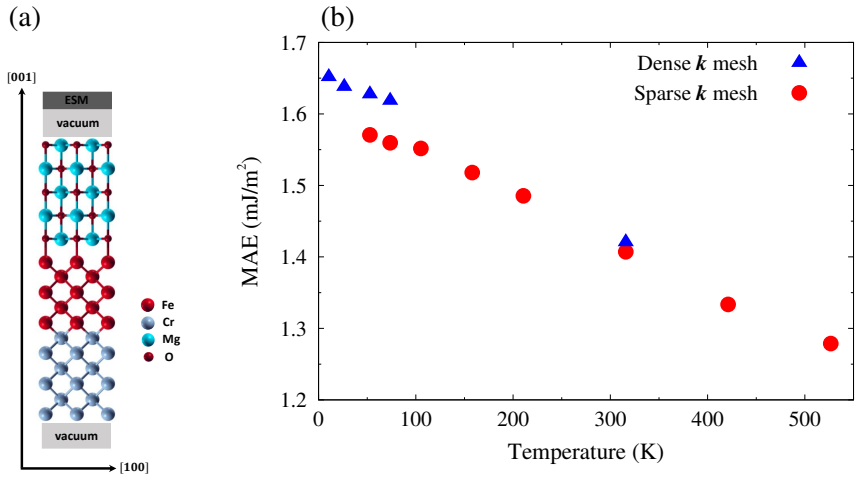

Figure 1: (a) Computational slab system equipped with an effective screening medium (ESM), and (b) Fermi level smearing effect in magnetic anisotropy energy (MAE) with respect to temperature. The symbols of triangle and circle specify the data by dense and sparse meshes, respectively.

field) arising from the other magnetic moments. This effect is taken into account partially in ε_i and ΔF. The magnetic dipole-dipole interaction between electrons, contributing to the SA, is included in ΔF.

In magnetic metals, the magnetic anisotropy largely depends on the details of electronic structures at the Fermi level. The theory of force theorem [26] clearly indicates that the one-particle energy ε_i plays an important role in the estimation of magnetic anisotropy. As also indicated at the first term in Eq. (2.1) the anisotropy energy may vary with the electron occupation f_i which smears the Fermi level as temperature increases. This smearing effect becomes large in case of the electronic structure which has a set of flat bands (spiky in the one-particle density of states) at the Fermi level. In particular, such feature can be found in low dimensional systems. In the demonstration shown later, the system has fine electronic structures in the energy width with several times of $k_B T_r$ (T_r: room temperature) at the Fermi level. The approach along the free energy of Eq. (2.1) needs an appropriate additional treatment to fully include the spin fluctuations of both transverse and longitudinal components when discussing the temperature dependence of magnetization [18, 19, 27].

2.2 Practical approach

The magnetic anisotropy also depends on the magnetic moment. As temperature increases, the magnetic moment decreases, and thus the anisotropy energy often decreases. The main part of such reduction may be realized by the contribution of SA. The temperature dependence of the magnetic moment originates from the spin fluctuations. In order to evaluate it, one can take a method based on the microscopic electronic structure [18,19]. However, for focusing the smearing effect at the Fermi level and for simplicity, this work employs a well-known sophisticated model as the temperature-dependent magnetization $M(T)$, as follows:

$$M(T) = M_0\, y(T/T^*), \tag{2.3}$$

where y is a given function, $M_0 = M(0)$, and T^* is a sophisticated parameter, such as Curie temperature (T_c). T^* is used as a sort of fitting parameters. In this work, due to the thinner magnetic

slab, we employed $y(T/T^*) = 1-(T/T^*)^2$ [24].

The magnetic anisotropy energy is presented as

$$K = K_{\rm b} + K_{\rm sa}, \tag{2.4}$$

where $K_{\rm b}$ is from the band energy and $K_{\rm sa}$ from the SA. $K_{\rm b}$ is expressed as the energy difference of free energy $F_{\rm b}$ between the different magnetization directions, such as [100](x-direction) and [001](z-direction) [28]. The $F_{\rm b}$ is given as follows [29, 30] :

$$F_{\rm b} = \sum_{n\mathbf{k}} f_{n\mathbf{k}}\left(\varepsilon_{n\mathbf{k}} - \mu\right) - k_{\rm B}TS + E_{\rm d} + \mu N_e\,, \tag{2.5}$$

where $E_{\rm d}$ is the double counting term in the total energy [26]. Using Eq. (2.5),

$$K_{\rm b} = F_{\rm b}^{[100]} - F_{\rm b}^{[001]}. \tag{2.6}$$

$K_{\rm sa}$ is expressed as

$$K_{\rm sa} = -\mu_0 M^2/2\Omega + \Delta K_{\rm sa}^{\rm int}, \tag{2.7}$$

where Ω and μ_0 are the volume of magnetic slab and permeability of vacuum, respectively, and $\Delta K_{\rm sa}^{\rm int}$ is the interface contribution which is not included in the 1st term. $\Delta K_{\rm sa}^{\rm int}$ originates from both the discreetness of stacking atomic layers [31] and the deviation from spherical atomic spin moment density at the interface magnetic atoms [32]. These are due to the shape of magnetization distribution, reducing the in-plane SA in ferromagnetic Fe layers.

2.3 Computational system

In the demonstration, we used the slab system, vacuum(0.79nm)/Cr(6ML)/Fe (5ML)/MgO(5ML)/vacuum(0.79nm) (ML=atomic monolayer) [see Fig. 1 (a)]. At the Fe/MgO interface the Fe atom was placed just next to the O atom due to its stability, and in the Cr and Fe layers the body-centered layer-stacking sequence was used. The in-plane lattice constant extracted from bulk Cr was employed. The effective screened medium (ESM) was introduced as an ideal metal. It is for avoiding an artificial electric field caused by the periodic boundary condition along the [001] direction [33]. The density functional calculation employs a fully relativistic (with spin-orbit interaction) ultrasoft pseudopotentials and planewave basis [34], by using the generalized gradient approximation [35]. We used a $32 \times 32 \times 1$ (sparse) mesh for the $\mathbf{k}$ point sampling in the estimations of $K_{\rm b}$. At the low temperatures, unfortunately, the sparse mesh mentioned above cannot give any convergence in the self-consistent calculation, and a $64 \times 64 \times 1$ (dense) mesh was also introduced. The difference from the sparse mesh appeared at the low temperatures, such as less than or equal to 100-200 K, and becomes small at 300 K. The dense mesh requires a large amount of computational source so that the number of calculated temperature points were limited to a few.

3 Result and Discussion

3.1 Magnetic anisotropy from spin-orbit interaction

Figure 1(b) shows $K_{\rm b}$ per unit area as a function of T. These values are positive, contributing to a perpendicular magnetic anisotropy as expected in a family of Fe/MgO interfaces [2, 3, 36], and

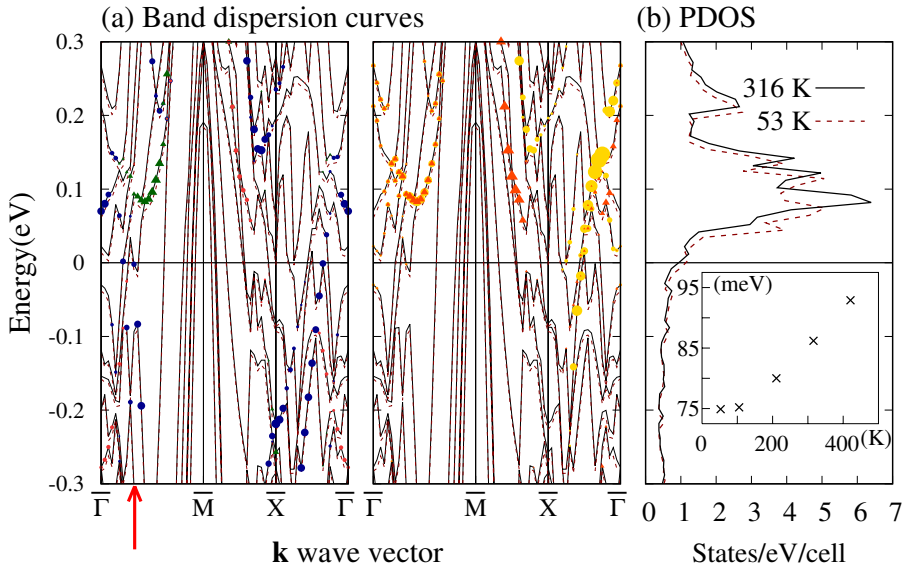

Figure 2: (a) Band dispersion curves (left and center) and (b) partial density of states (right) for the minority-spin-state 3d orbital on the interface Fe in the [001] magnetization system determined with the temperature-dependent Fermi level smearings of 316 K (full curves and symbols) and 52.8 K (broken curves). The symbols specify the angular orbital components projected on the interface Fe atoms; $d_{xy}, d_{x^2-y^2}, d_{3z^2-r^2}$(left) in blue, green, and red bullets, respectively, and d_{xz}, d_{yz} (center) in orange and yellow. The Fermi levels are adjusted to zero in the vertical axis with the horizontal full line, and the Fermi energy (chemical potential μ) decreases by 0.11 eV as temperature. The inset figure in (b) shows the typical data of $\varepsilon_{n\mathbf{k}} - \mu$ with respect to the temperature at $\mathbf{k} = 0.33 \times \bar{\Gamma}\bar{\mathrm{M}}$ (vertical red arrow).

similar to the data (1.5 mJ/m^2) from the experimental measurement at the room temperature for the Fe thickness (t_{Fe}) of 0.7nm [12]. Such positive contribution may be attributed to the SOCs between the orbital components of d_{xy} and $d_{x^2-y^2}$, or d_{xz} and d_{yz} in the respective occupied and unoccupied states [37]. The smearing effect decreases K_{b} monotonically by 0.38 mJ/m^2 from 10.5 K to 527 K. This decreasing quantity is not negligible, implying one of important ingredients for the temperature dependence of magnetic anisotropy.

3.2 Electronic structure

K_{b} decreasing with temperature is a consequence of electronic structure. To confirm the variation property, in Fig. 2 we show the band dispersion curves and the partial density of states (PDOS) for two different temperatures (52.8 K and 316 K). The eigenvalue with respect to the chemical potential ($\varepsilon_{n\mathbf{k}} - \mu$) is increased roughly by 0.01 eV in almost all the Brillouin zone. In particular, focusing the unoccupied states dominated by 3d orbitals at around 0.09 eV, the eigenvalue tends to behave $(\varepsilon_{n\mathbf{k}} - \mu) = \varepsilon^0_{n\mathbf{k}} - \mu_0 + \alpha T^2$, where $\varepsilon^0_{n\mathbf{k}}$ and μ_0 are the eigenvalue and chemical potential, respectively, extrapolated to 0 K, and α is a positive constant (typical temperature dependence of $\varepsilon_{n\mathbf{k}} - \mu$ is shown in the inset of Fig. 2). Consequently, the quantity of $1/(\varepsilon_{n\mathbf{k}} - \mu)$ decreases as temperature, implying a decrease in K_{b} considering the second-order perturbation formula for spin-orbit interaction [37]. In the present case, the α is small so that $\alpha T^2/(\varepsilon^0_{n\mathbf{k}} - \mu_0)$ is much smaller than the unity, showing a gradual temperature dependence in K_{b} like a linear, instead of a complicated dependence. Quantitatively the decreasing rate by the Fermi level smearing should

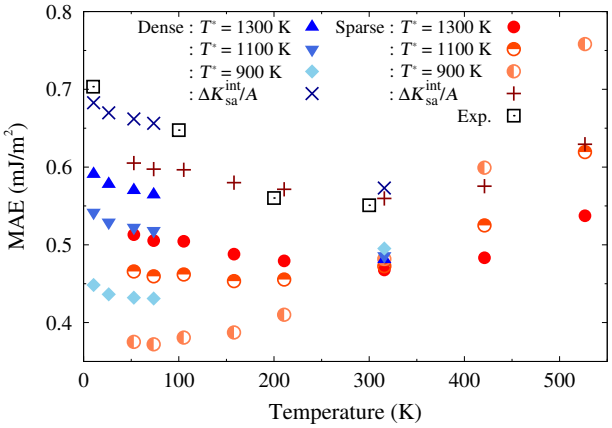

Figure 3: Total magnetic anisotropy energy (K) per unit area with respect to temperature. The symbols of triangle, bullet, circle, diamond indicate the data of $T^* = 900, 1100, 1300$K for $\Delta K_{sa}^{int} = 0$ and those of cross and plus for $T^* = 1300$K and $\Delta K_{sa}^{int}/A = 0.09$mJ/m^2, where A is the interface area. The empty square symbols specify the experimental data extracted from reference [10].

be canceled out partially by the other contributions so as to showing a gradual decline such as observed in the experimental measurement [10].

3.3 Including shape magnetic anisotropy

In order to validate the smearing effects obtained above comparing them with the experimental results, we had performed a simulation on K using the parameters of M_0 and T^*. In this simulation we used the Fe layer thickness ($t_{Fe} = 0.710$nm). This t_{Fe} is comparable to those obtained by the first-principles calculation. As a result the M_0 can be fixed to the value which reproduces the experimental magnetization at 300 K ($M(300\text{K}) = 1.83$ T [38]) [11]. We also found that, comparing the results of the T^*s of 800, 900, 1000, 1100, 1200, 1300, and 1400K, the T^*s between 1200K and 1300K give a reasonable fitting to the temperature dependence of available experimental data [10] except a temperature-independent value implying ΔK_{sa}^{int}. In Fig. 3, the total K per area are plotted as temperature for the parameters of $T^* = 900$K, 1100K, and 1300K, where $\Delta K_{sa}^{int} = 0$. At the lower T^*s, the in-plane SA becomes larger and the difference from the experimental data also becomes large at the low temperatures.

In Fig. 3, the total K per unit area is also shown for a non-zero ΔK_{sa}^{int}. This plot implies that, assuming the interface contribution of SA ($\Delta K_{sa}^{int}/A = 0.09$mJ/m^2), K becomes close to the experimental results. This quantitative assumption in ΔK_{sa}^{int} is not so far from a realistic contribution, because the quadrupole atomic spin density of prolate type at the interface can reduce the in-plane SA by an energy comparable to that in the free-standing Fe 1ML (0.10mJ/m^2) [32]. Note that such contribution does not depend on the total magnetization. On the fitting to another experimental data of $M(300\text{K}) = 2.09$T [12], the set of parameters ($\Delta K_{sa}^{int}/A = 0.35$mJ/m^2, $T^* = 1400$K) provides a reasonable temperature dependence in K (see Appendix). This parameter of ΔK_{sa}^{int} is not too large, because the parameter originates from both interfaces in the Fe layer. Further investigations on the origin of ΔK_{sa}^{int} are required for analyzing real magnetic interfaces.

Our analysis on the temperature dependence of K can predict a behavior at the higher temperatures. As shown in Fig. 3, our result indicates that it increases as temperature increases after

some temperature. Note that such behavior is a consequence that as temperature increaces, the perpendicular K_b decreases and the in-plane SA ($|K_{sa}|$) also decreases more rapidly with a growth of spin fluctuations. The behavior that the SA works as an enhancement of PMA or as a suppressing origin in the reduction of PMA at higher temperatures, may be one of important general interests in the thin ferromagnetic materials. Note that at further higher temperatures near T_c the Mermin's approach is no longer useful and should be corrected in accordance with existing large spin-fluctuations [27]. In a further general treatment on magnetic anisotropy, temperature effects originating from a magnetoelastic anisotropy should be considered.

In our analysis, the parameter of T^* is relatively flexible, compared with the other parameter of M_0. T^* around 1300K seems to be suitable to explain the available experimental data. If T^* is regarded as T_c, this T_c (= 1300K) is comparable to those of bcc Fe (T_c = 1043K). When considering a T_c formula in the approach of localized spin moment, T_c is proportional to both the exchange coupling constant and the square of magnetization. Roughly speaking, the effective T_c may increase, because the magnetic moments on Fe atom tend to be enhanced at the interfaces. Further information on T_c should be required in the computational approach as well as in the approaches of phenomenological theory and experimental measurement.

Our present approach to a temperature dependent MAE may indicate a correspondence with an available experimental data. However, it is still unclear that the spin fluctuation at finite temperatures is fully considered. This is because the electronic structure calculation, which is a basis of the MAE originating from the spin-orbit interaction, does not include effects of finite temperature in the atomic spin configuration, while the spin configuration at finite temperatures should be an ensemble of various directions for atomic magnetic moments. The last picture is a reason why the strength of total magnetization tends to decrease as temperature increases. An improved approach to MAE estimation is required for a computational material design of magnetic materials.

4 Summary

We performed the first-principles calculations on the MAE from the band energy contribution using the temperature-dependent Fermi level smearing in the Fe(5ML)/MgO slab. The contribution of the MAE decreases by 0.4 mJ/m^2 as temperature from 10.5K to 527K. When employing the simple formula for the SA and assuming the experimental saturated magnetization with the appropriate temperature dependence for ultra-thin films, the total MAE shows a nearly flat part around the room temperature. This theoretical analysis may predict an increase of the perpendicular total MAE at higher temperatures. Such increase may be a possible general consequence of the balance between a large perpendicular band energy contribution and small in-plane shape anisotropy. The present work provides a new pathway to understand origins of a temperature dependence in MAE.

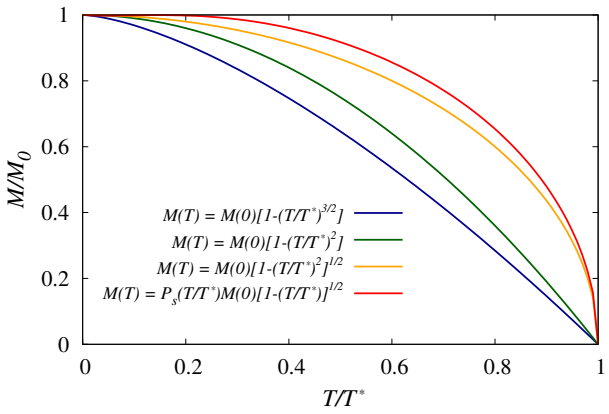

Figure 4: Reduced magnetization, M/M_0 as a function of reduced temperature T/T^*.

A Appendix: Simulation on shape anisotropy

The reduced magnetization, $M(T)/M(0)$, is expressed as a function of the reduced temperature, T/T^*. In the simulations on SA, we tried to choose the following functions [22, 24, 39, 40] :

$$M(T) = M(0)\left[1-\left(\frac{T}{T^*}\right)^2\right], \tag{A.1}$$

$$M(T) = M(0)\left[1-\left(\frac{T}{T^*}\right)^{3/2}\right], \tag{A.2}$$

$$M(T) = M(0)\left[\sqrt{1-\left(\frac{T}{T^*}\right)^2}\right], \tag{A.3}$$

$$M(T) = P_S\left(\frac{T}{T^*}\right)M(0)\left[\sqrt{1-\left(\frac{T}{T^*}\right)}\right], \tag{A.4}$$

where

$$\begin{aligned} P_S(T/T^*) \quad = \quad & \left[1+0.410721(T/T^*)+1.65224(T/T^*)^2-5.60792(T/T^*)^3+9.67475(T/T^*)^4\right. \\ & \left.-9.30572(T/T^*)^5+4.74404(T/T^*)^6-1.00258(T/T^*)^7\right]. \end{aligned} \tag{A.5}$$

These functions are shown in Fig. 4. Using the assumed function of $M(T)$, the Total MAE (K) as a function of temperature is fitted to an experimental data [10]. $M(0)$ was determined so as to reproduce an experimentally measured magnetization at 300K; $M(300K) = 1.83$T [11] and 2.09T [12] were used in Figs. 5 and 6, respectively.

The total magnetic anisotropy for each $M(T)$ function is presented in Fig. 5, compared with the experimental data extracted from Xiang et al. [10]. The functions of Eqs. (A.1), (A.2), (A.3), and (A.4) are used in Figs. 5 (a), (b), (c), and (d), respectively, with the experimental magnetization [M(300K)=1.83T] extracted from Ref. [11]. Various T^*s were used from 800 to 1400K. In Fig. 5, the resulting data are presented only for 900, 1100, and 1300K. The choice of the first $M(T)$ function (which is proportional to T^2) could reproduce the tendency of experimental data, especially for the case of T^*=1300K. The flat part of total MAE is remarkably reproduced when the temperature increases from 200K to 300K. As shown in Fig. 5 (a), the choice of lower T^* gives an

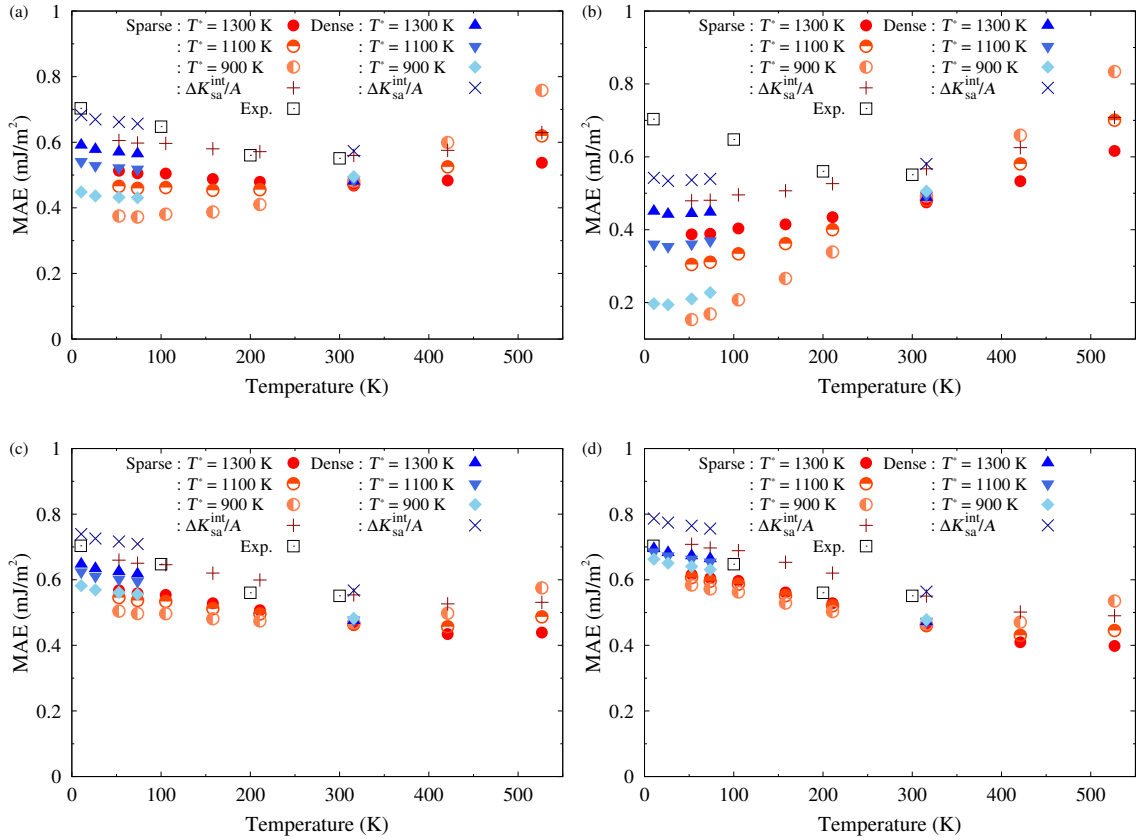

Figure 5: Total magnetic anisotropy energy (K) per unit area with respect to temperatures; (a), (b), (c), and (d) for the functions in Eqs. (A.1), (A.2), (A.3) and (A.4), respectively. The symbols of triangle, bullet, circle, diamond indicate the data of T^* = 900, 1100, 1300K for $\Delta K_{\rm sa}^{\rm int} = 0$ and those of cross and plus for T^* = 1300K and $\Delta K_{\rm sa}^{\rm int}/A = 0.09$mJ/m^2, where A is the interface area. The empty square symbols specify the experimental data extracted from Ref. [10]. The experimental magnetization [M(300K)=1.83T] extracted from Ref. [11].

increasing tendency of total MAE as the temperature increases. These features are not favorable, compared with the experimental tendency. When we choose the second $M(T)$ function presented at Eq. (A.2), the total MAE at low temperature is largely underestimated and increases linearly as the temperature increases. The total MAE from the third $M(T)$ function gives a reasonable comparison with the experimental data. However, this choice of function and set of parameters tends to show a different trend at the flat part around 200K and 300K of experimental data. The choice of the fourth $M(T)$ function gives an overestimation at low temperatures, compared with the experimental data and also gives a linear decreasing tendency as the temperature increases. At high temperatures it provides a lower total MAE, compared to other three functions. This $M(T)$ function cannot also reproduce the behavior around 200K and 300K in the experimental data. From the simulation presented in Fig. 5, the first $M(T)$ function (A.1) with T^* of 1300K may provide an acceptable result reproducing the experimental data.

Next, another experimental magnetization is considered. The total magnetization of M(300K)= 2.09T is extracted from Koo et al. [12]. The results of simulation are presented in Fig. 6, as for the magnetization of 1.83T. This total magnetization largely underestimates all of our data in the total MAE. The best result is provided by the first $M(T)$ function with T^*=1400K. This result

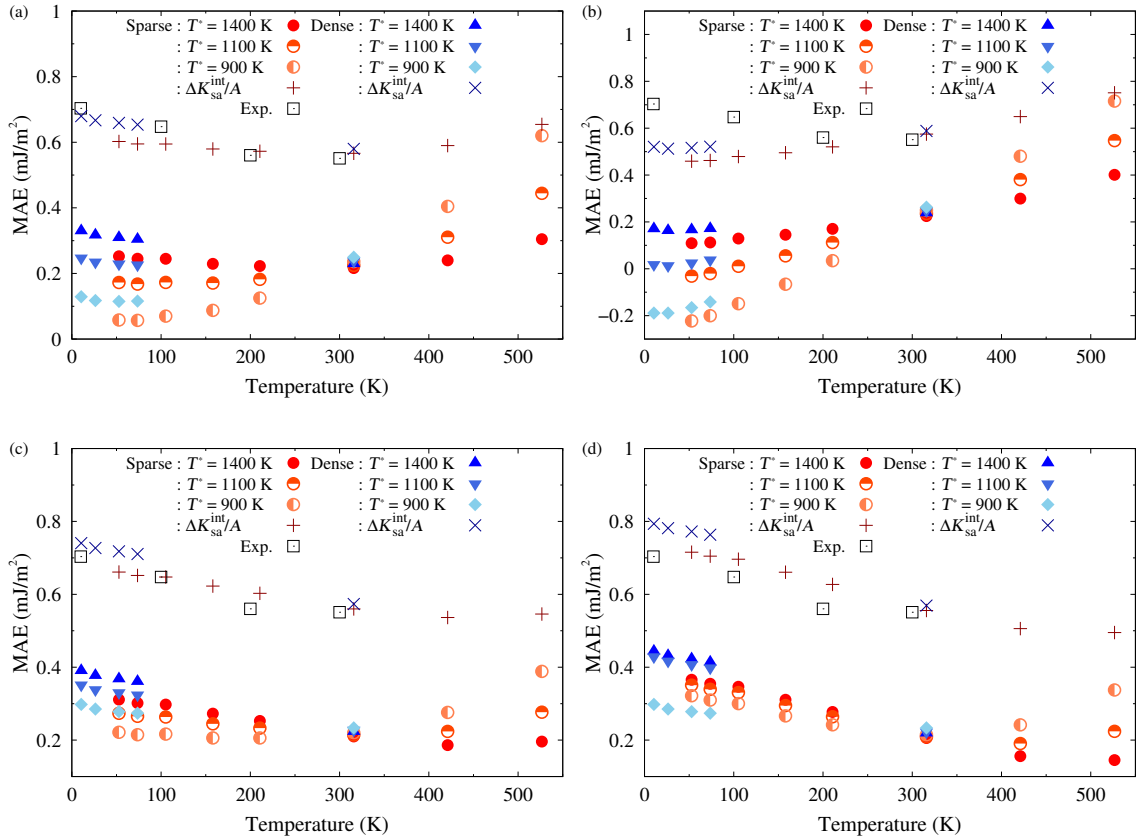

Figure 6: Same quantities (K per unit area) as in Fig. 5 with the different parameters. The symbols of triangle, bullet, circle, diamond indicate the data of T^* = 900, 1100, 1400K for $\Delta K_{\rm sa}^{\rm int} = 0$ and those cross and plus for T^* = 1400K and $\Delta K_{\rm sa}^{\rm int}/A = 0.35$mJ/m^2. The experimental magnetization [M(300K)=2.09T] extracted from Ref. [12].

may reproduce the behavior around 200K and 300K in the experimental data when we choose $\Delta K_{\rm sa}^{\rm int}/A = 0.35{\rm mJ/m}^2$ as the interface anisotropy. In the simulations of Fig. 5 and Fig. 6, we introduced $\Delta K_{\rm sa}^{\rm int}/A = 0.09{\rm mJ/m}^2$ and $\Delta K_{\rm sa}^{\rm int}/A = 0.35{\rm mJ/m}^2$, respectively. Although the fabricated systems are different between Nozaki et al. [11] and Koo et al. [12], those magnetic slabs are similar to each other. The difference in $\Delta K_{\rm sa}^{\rm int}/A$ should be explained with a reasonable origin in future.

B Appendix: Magnetic moments of density functional approach

The magnetic moments obtained by the density functional approach are displayed for typical temperatures of 53K (sparse mesh) and 316K (sparse mesh) in Table 1 and Table 2. These data were estimated from the spin density by integrating it in the atomic sphere with the radius (Fe: 1.32Å, Cr: 0.90Å).

Table 1: Spin magnetic moments in μ_B on Cr and Fe atoms. The temperature specifies the value used in the Fermi level smearing. [001](z-direction) and [100](x-direction) specify the direction of total magnetization.

Temperature	Total	Fe(1)	Fe(2)	Fe(3)	Fe(4)	Fe(5)
53K [001]	12.7964	2.8481	2.5311	2.5984	2.4986	2.3202
53K [100]	12.7964	2.8499	2.5295	2.5975	2.4992	2.3203
316K [001]	12.7844	2.8420	2.5286	2.5960	2.5008	2.3170
316K [100]	12.7848	2.8428	2.5286	2.5957	2.5007	2.3170

Temperature	Cr(1)	Cr(2)	Cr(3)	Cr(4)	Cr(5)	Cr(6)
53K [001]	-1.0678	0.9999	-1.0902	1.2247	-1.4434	2.3329
53K [100]	-1.0674	0.9999	-1.0903	1.2245	-1.4433	2.3330
316K [001]	-1.0689	0.999	-1.0905	1.2209	-1.4421	2.3309
316K [100]	-1.0689	0.9989	-1.0906	1.2208	-1.4421	2.3308

Table 2: Orbital magnetic moments in μ_B on Cr and Fe atoms. The temperature specifies the value used in the Fermi level smearing.

Temperature	Total	Fe(1)	Fe(2)	Fe(3)	Fe(4)	Fe(5)
53K [001]	0.29061	0.08476	0.05967	0.05076	0.05301	0.04241
53K [100]	0.25549	0.06251	0.04822	0.04944	0.05068	0.04464
316K [001]	0.2855	0.0833	0.0574	0.0498	0.0524	0.0427
316K [100]	0.2572	0.0649	0.0478	0.0492	0.0505	0.0448

Temperature	Cr(1)	Cr(2)	Cr(3)	Cr(4)	Cr(5)	Cr(6)
53K [001]	0.00996	-0.00612	0.00935	-0.00746	0.0105	-0.01491
53K [100]	0.01182	-0.00607	0.00888	-0.00911	0.00931	-0.02182
316K [001]	0.0098	0.0062	0.0094	0.0075	0.0105	0.0150
316K [100]	0.0121	0.0062	0.0091	0.0090	0.0093	0.0211

C Appendix: MAE from Bruno's relation

One can estimate MAEs from the orbital magnetic moments by using Bruno's formula [41]

$$\mathrm{MAE} = \xi \frac{m_{\mathrm{o}}^{[001]} - m_{\mathrm{o}}^{[100]}}{4\mu_{\mathrm{B}}}, \tag{C.1}$$

where ξ is the spin-orbit coupling constant (Fe: 51 meV/atom) and $m_{\mathrm{o}}^{[001]}$ ($m_{\mathrm{o}}^{[100]}$) is the orbital magnetic moment for the [001] ([100]) magnetization direction. The MAE was estimated for each atom and displayed with the total for the typical temperature in Table 3. The totals are underestimated compared with the respective values indicated in Fig. 1(b) in the main text. These underestimation may be attributed to the details of 3d-orbital hybridization on Fe atom around the Fermi level. Interestingly, the difference between 53K and 316K on the total MAE is very similar to the corresponding value indicated in Fig. 1(b) in the main text.

Table 3: Magnetic anisotropy energy (mJ/m^2) of Bruno's formula estimated from the orbital moments shown in Table. 2.

Temperature	Total	Fe(1)	Fe(2)	Fe(3)	Fe(4)	Fe(5)
MAE(53K)	0.87	0.55	0.28	0.03	0.06	-0.06
MAE(316K)	0.70	0.45	0.24	0.01	0.05	-0.05
difference	0.17	0.10	0.04	0.02	0.01	-0.01

Acknowledgements

The first-principles calculations were performed using the facilities of the Supercomputer Center, Institute for Solid State Physics, the University of Tokyo, Japan. This work was partly supported by Grant-in-Aid for Scientific Research from JSPS/MEXT (Grant Nos. 15K05165 and 18K04923). This research partly used computational resources of the K computer and other computers of the HPCI system provided by the AICS and Information Technology Center of Nagoya University through the HPCI System Research Project (Project ID:hp160107, hp160227, hp170168). This work was partly supported by the ImPACT Program of Council for Science, Technology and Innovation (Cabinet Office, Japan Government), and by the Computational Materials Science Initiative (CMSI), Japan. The authors (N.I and I.P.) acknowledges Japanese Government (MEXT) Scholarship in the Program for the Development of Global Human Resources for Kanazawa University.

References

[1] H. Ohno, Nat. Mater. **9**, 952 (2010).

[2] S. Ikeda, K. Miura, H. Yamamoto, K. Mizunuma, H. D. Gan, M. Endo, S. Kanai, J. Hayakawa, F. Matsukura, and H. Ohno, Nat. Mater. **9**, 721 (2010).

[3] T. Nozaki, Y. Shiota, T. Shinjo, and Y. Suzuki, Appl. Phys. Lett. **96**, 022506 (2010).

[4] M. Endo, S. Kanai, S. Ikeda, F. Matsukura, and H. Ohno, Appl. Phys. Lett. **96**, 212503 (2010).

[5] C. G. Duan, J. P. Velev, R. F. Sabirianov, Z. Zhu, J. Chu, S. S. Jaswal, and E. Y. Tsymbal, Phys. Rev. Lett. **101**, 137201 (2008).

[6] K. Nakamura, R. Shimabukuro, Y. Fujiwara, T. Akiyama, T. Ito, and A. J. Freeman, Phys. Rev. Lett. **102**, 187201 (2009).

[7] T. Maruyama, Y. Shiota, T. Nozaki, K. Ohta, N. Toda, M. Mizuguchi, A. A. Tulapurkar, T. Shinjo, M. Shiraishi, S. Mizukami, Y. Ando, and Y. Suzuki, Nat. Nanotechnol. **4**, 158 (2009).

[8] Y. Shiota, T. Nozaki, F. Bonell, S. Murakami, T. Shinjo, and Y. Suzuki, Nat. Mater. **11**, 39 (2012).

[9] Y. Hibino, T. Koyama, A. Obinata, T. Hirai, S. Ota, K. Miwa, S. Ono, F. Matsukura, H. Ohno, and D. Chiba, Appl. Phys. Lett. **109**, 082403 (2016).

[10] Q. Xiang, Z. Wen, H. Sukegawa, S. Kasai, T. Seki, T. Kubota, K. Takanashi and S. Mitani, J. Phys. D: Appl. Phys. **50**, 40LT04 (2017).

[11] T. Nozaki, A. Kozioł-Rachwał, W. Skowroński, V. Zayets, Y. Shiota, S. Tamaru, H. Kubota, A. Fukushima, S. Yuasa, and Y. Suzuki, Phys. Rev. Appl. **5**, 044006 (2016).

[12] J. W. Koo, H. Sukegawa, S. Kasai, Z. C. Wen, and S. Mitani, J. Phys. D: Appl. Phys. **47**, 322001 (2014).

[13] J. Kanamori, "Anisotropy and Magnetostriction of Ferromagnetic and Antiferromagnetic Materials", in Magnetism Volume 1 (H. Suhl and G. T. Rado, Academic Press, New York, 1963) Chap. 4, p. 127.

[14] E. R. Callen and H. B. Callen, J. Phys. Chem. Solids **27**, 1271 (1966).

[15] Y. Millev and M. Fähnle, Phys. Rev. B, **52**, 4336 (1995).

[16] J.-U. Thiele, K. R. Coffey, M. F. Toney, J. A. Hedstrom, and A. J. Kellock, J. Appl. Phys. **91**, 6595 (2002).

[17] S. Okamoto, N. Kikuchi, O. Kitakami, T. Miyazaki, Y. Shimada, and K. Fukamichi, Phys. Rev. B **66**, 24413 (2002).

[18] O. N. Mryasov, U. Nowak, K. Y. Guslienko, and R. W. Chantrell, Europhys. Lett. **69**, 805 (2005).

[19] J. B. Staunton, S. Ostanin, S. S. A. Razee, B. L. Gyorffy, L. Szunyogh, B. Ginatempo, and E. Bruno, Phys. Rev. Lett. **93**, 257204 (2004).

[20] I. A. Zhuravlev, V. P. Antropov, and K. D. Belashchenko, Phys. Rev. Lett. **115**, 217201 (2015).

[21] J. G. Alzate, P. K. Amiri, G. Yu, P. Upadhyaya, J. A. Katine, J. Langer, Appl. Phys. Lett. **104**, 112410 (2014).

[22] F. Blöch, Z. Phys. **61**, 10.1007 (1930).

[23] Z. Wen, H. Sukegawa, T. Seki, T. Kubota, K. Takanashi, and S. Mitani, Sci. Rep. **7**, 45026 (2017).

[24] U. Köbler, J. Phys.: Condens. Mater **14**, 8861 (2002).

[25] N. D. Mermin, Phys. Rev. **137**, A1441 (1965).

[26] G. H. O. Daalderop, P. J. Kelly, M. F. H. Schuurmans, and F. Jansen, Phys. Rev. B **41**, 11919 (1990).

[27] A. Buruzs, P. Weinberger, L. Szunyogh, L. Udvardi, P. I. Chleboun, A. M. Fischer, and J. B. Staunton, Phys. Rev. B **76**, 064417 (2007).

[28] M. Tsujikawa, A. Hosokawa and T. Oda, Phys. Rev. B **77**, 054413 (2008).

[29] M. Weinert and J. W. Davenport, Phys. Rev. B **45**, 13709 (1992).

[30] T. Oda, J. Phys. Soc. Jpn. **71**, 519 (2002).

[31] H. J. G. Draaisma and W. J. M. de Jonge, J. Appl. Phys. **64**, 3610 (1988).

[32] T. Oda and M. Obata, J. Phys. Soc. Jpn. **87**, 064803 (2018).

[33] M. Otani and O. Sugino Phys. Rev. B **73**, 115407 (2006).

[34] T. Oda and A. Hosokawa, Phys. Rev. B **72**, 224428 (2005).

[35] J. P. Perdew, J. A. Chevary, S. H. Vosko, K. A. Jackson, M. R. Pederson, D. J. Singh, and C. Fiolhais, Phys. Rev. B **46**, 6671 (1992).

[36] R. Shimabukuro, K. Nakamura, T. Akiyama, T. Ito, Physica E **42**, 1014 (2010).

[37] D.-S. Wang, R. Wu, and A. J. Freeman, Phys. Rev. B **48**, 15886 (1993).

[38] The unit of T ($\mathrm{Wb/m^2}$) is used for magnetization (M) in MKSA units: $1\mathrm{T} = 10^7/4\pi\,\mathrm{A/m}$ in the international system of units (SI), $1T = 10^4/4\pi\,\mathrm{emu/cm^3}$ in cgs-Gauss units.

[39] A. S. Arrot, J. Appl. Phys. **103**, 07C715 (2008).

[40] V. Barsan and V. Kuncser, Phil. Mag. Lett. **97**, 359 (2017).

[41] P. Bruno, "Physical origins and the theoretical models of magnetic anisotropy" in Lecture Notes, IFF Ferienkurs Magnetismus von Festköpern und Grenzächen 24 (P. H. Dedrichs, P.Grünberg and W. Zinn, Jülich). (1993) p.24.19.